

Contents lists available at ScienceDirect

Carbon Trends

journal homepage: www.elsevier.com/locate/cartre





Templating-induced graphitization of novolac using graphene oxide additives

Sandra N Ike a,b,*, Randy Vander Wal a,b

- ^a The John and Willie Leone Family Department of Energy and Mineral Engineering Penn State University, 16801, USA
- ^b EMS Energy Institute, Penn State University, 16801, USA

ARTICLE INFO

Keywords:
Reduced graphene oxide (RGO)
Graphene oxide (GO)
Novolac
Oxygen content
Templating, graphitization

ABSTRACT

Increasing graphite demand for energy storage applications creates the need to make graphite using precursors and processes that are affordable and friendly to the environment. Non-graphitizing precursors such as biomass or polymers are known for their low cost and sustainability; therefore, graphitizing them will be an accomplishment. In this work, a process of converting a non-graphitizing precursor, phenolic resin novolac (N), into a graphitic carbon is presented. This was achieved by the addition of five additives categorized as graphene oxide (GO) and its derivatives with varied oxygen concentrations. The hypothesis is that the additives act as templates that promote matrix aromatic alignment to their basal planes during carbonization (physical templating) in addition to forming radical sites that bond to the decomposing matrix (chemical templating). Results showed that the addition of reduced graphene oxide (RGO) additives of approximately 15.4 at.(%) oxygen content to the novolac matrix (RGO-N) show the best graphitic quality. In contrast, the addition of GO additive of twice or more oxygen content \geq 30.8 at.(%) to the novolac matrix (GO-N) led to poor graphitic quality. This suggests that there is an optimum amount of oxygen content in GO additives needed to induce graphitization of the novolac matrix.

1. Introduction

Graphitization is an energy intensive process. The Acheson process is still the preferred method for graphitization of carbon precursors. This process operates at temperatures above 2800 °C and requires a long processing time leading to the high cost of synthetic graphite [1]. The process utilizes precursors such as petroleum cokes and tar pitches which are graphitizable carbon precursors [2-7]. However, these precursors are unsustainable and come from polluting sources. With high demand for graphite in traditional applications such as electrodes in aluminum refining and electric arc furnaces steel industries and now with the forecasted exponential rise of electric vehicles [8-10] and associated lithium ion batteries, there is an urgent need to find cost-effective carbon precursors and alternative approaches for graphitization. For example, carbon precursors such as phenolic and furan resins and even biomaterials like lignin and sugar are of major interest because of the abundance, low cost, high carbon content, less pollution, sustainability of these precursors, and unique electronic and structural properties [11,12]. However, converting these non-graphitizable precursors into a highly ordered graphitic structure presents a challenge. Accompanying this challenge is interest in reducing the energy and cost associated with graphitization by using lower temperature.

Attempts to understand controlling factors on graphitization has stimulated different research works and many factors have been attributed to the cause of graphitization of non-graphitizable carbon matrices. In a study by Lanticse-Diaz et al., anisotropic structures were formed in the area around the carbon nanotubes (CNT) in a furan resin/ CNT carbon-carbon (C-C) composite after heat treatment at 2800 °C [13]. It was suggested that interaction between the furan resin matrix and CNT (diameter of 100-300 nm) at the interface prevents the matrix from shrinking during graphitization resulting in a stress gradient beyond the interface leading to stress graphitization. Upon analysis, stress-induced graphitization assumes the following: First, wetting of the carbon nanotube by the matrix and, second, a perpendicular (stress-induced) force that propagates to some degree to cause matrix restructuring into a graphitic form. However, it is unclear how and why the matrix retains sufficient integrity to propagate such a stress during severe pyrolysis and decomposition. Originally the concept emerged from observations with continuous fiber composites wherein the extended fibers were considered to resist matrix contraction [14]. However, for MWCNT with variable curvature, twists, and bends, it is unclear how such stress develops over straight-lengths of a few 10's of nanometers.

^{*} Corresponding author at: The John and Willie Leone Family Department of Energy and Mineral Engineering Penn State University, 16801, USA. *E-mail address:* sxi5097@psu.edu (S.N. Ike).

The explanation seems to relate the internal change of a matrix, namely formation of graphitic structure, to an extrinsic physical constraint such as the boundary of carbon fibers or nanocarbon additives. Tzeng et al. [15], studied a CNT reinforced phenolic resin C—C composite and observed the formation of graphitic rods at 2000 °C. Also, in a study done by Nam et al., acid treated CNT were dispersed into a polyaniline (PANI) matrix and heat treated at temperatures above 1500 °C. They observed crystalline structures in the composites heated to 1700 °C. It is important to note that the temperatures at which graphitic structures were observed in these studies is far below the temperature reported for stress graphitization as proposed by Lanctice-Diaz et al. [13].

In related work, Saha et al. [16], explored the templating ability of nanomaterials, CNT and graphene, in the graphitization of polyacrylonitrile derived fibers (PAN) using reactive force field (ReaxFF) and molecular dynamics (MD). Depending on temperature, two mechanisms were proposed for graphitization: physisorption and chemisorption. The former, referred to here as "physical templating", occurred as temperature approached 2200 K (\sim 1900 °C) where templating is governed by π $-\pi$ interactions between the π -conjugated system of the nanofillers and π -electrons of the C \equiv N groups and/or all the carbon rings of the PAN fibers. The latter chemisorption, referred to here as "chemical templating", occurred as temperature approaches 3000 K (~2700 °C) where functional groups such as C≡N on the carbon matrix become 'leaving groups' and form radical sites for covalent bonding with the nanofiller. Gao et al. [17] also used atomistic ReaxFF and large-scale MD simulations to explain the mechanism by which graphene could modify the microstructure in graphene reinforced carbon fibers. This study found that there are dangling bonds on the graphene edges, which form bonds with the polymer matrix, serving as "catalytic seeds" for the formation of larger graphitic structure. Ma et al. [18] reported an increase in graphitization in a carbon/phenolic resin C-C composite reinforced with graphene oxide (GO). Their MD simulations showed that even small concentrations of GO served as a nucleating agent for the formation of graphitic structure. These authors found that the oxygen-containing functional groups on the GO play a significant role in enhancing the interfacial reactions between the GO and phenolic resin matrix. To date there is yet little experimental study on this theory to understand the role of oxygen functional groups in graphene additives and its influence in graphitization behavior of a non-graphitizable carbon matrix. Different studies have been conducted and have ascribed varied causes (stress, strain, physical and chemical templating) to the observed graphitization of hard carbon matrices/precursors. Presently, mechanistic understanding is lacking by which these factors induce graphitization, let alone ranking. Another drawback is that there is no experimental work to provide a basis for (or validation of) modeling studies for the oxygen content of additives upon templating of non-graphitizing carbon precursors. Moreover, the contributions and balance between oxygen content and sp² framework upon graphitization remain untested. These knowledge gaps motivated the current study.

In this work, the effect of templating using graphene oxide (GO) additives to graphitize novolac (a non-graphitizing precursor) was demonstrated. These additives were selected based on their varied oxygen content. The hypothesis is that the oxygen functional groups of the GO additives would act as leaving groups and form radical sites for bonding and alignment with matrix radicals during heat temperature treatment (HTT). This process is referred to as *chemical templating*. Furthermore, the aromatic rings derived from the novolac matrix interact with the $\rm sp^2$ network of the two-dimensional nanomaterials (as identified by the ReaxFF based study [16,17], thereby aiding in formation of layered graphite material, a process referred to as *physical templating*.

2. Experimental methods

2.1. Preparation of novolac

Novolac was prepared with phenol to formaldehyde molar ratio less than one using concentrated hydrochloric acid (HCl) as a catalyst. The resulting solution was stirred with a magnetic stirrer and heated to approximately 70 $\,^{\circ}\text{C}$ as the phenol dissolved. Once the phenol completely dissolved, 5 ml of concentrated HCl was added in drops using a pipette. After a few minutes, polymerization reaction was visible as the solution began to change from a clear to a milky color followed by a spontaneous and dramatic bubble rise in the beaker. A whitish-pink precipitate then formed.

2.1.1. Addition of graphene oxide derived additives

Five graphene oxide-derived additives (Table 1) were selected as templating agents: two graphene oxides (GO), two reduced graphene oxides (RGO) and a graphene nanoplatelet (GPL). GPL (5.3 at.(%) O), RGO (14.4 at.(%) O) and GO (30.8 at.(%) O) materials were gotten from the vendor, Cheap Tubes. RGO (15.4 at.(%) O) was obtained from the graphene supermarket and GO (35.3 at.(%) O) was purchased from Abalonyx. All additives were used as received from the vendors. A predetermined weight percentage of each was first dispersed into methanol and sonicated for six minutes. Novolac (N) with each additive was then left to mix and stir overnight resulting in a thick viscous black liquid or semi-solid with clay-like consistency. See supporting information for XPS and TEM characterizations of additives.

2.1.2. Carbonization

Carbonization was done in a customized pressurized tubing reactor. The sample was wrapped in brass foil and inserted into the reactor. The reactor was then pressurized with nitrogen to purge out oxygen and checked for leaks. Carbonization was done at $500\,^{\circ}\text{C}$ for 5 h. The pressure in the reactor typically ranges between $500\,$ and $1500\,$ psi during the carbonization process. After carbonization is completed, the reactor is allowed to cool down, opened, and the carbonized sample is collected for subsequent graphitization.

2.1.3. Graphitization

Carbonized samples were weighed, placed in graphite crucibles, and put into a Centorr Vacuum Industries series 45 graphitization furnace. Graphitization was performed at 2500 $^{\circ}\text{C}$ for 1 h under the argon atmosphere.

2.2. Characterization

2.2.1. X-ray diffraction (XRD)

The X-ray diffraction patterns were collected using Malvern PANalytical Empyrean diffractometer equipped with Cu source ($\lambda\cong1.54A^\circ$), para-focusing optics and PIXcel 3D detector. The spectrum was scanned in the 2θ range of $10^\circ-90^\circ$. The background subtraction, peak fitting and quantification were done using MDI JADE® software. Lattice parameters were calculated with the following formula:

Table 1
Summary of additive oxygen content (at.%) measured by XPS.

% Additive carbon content	% Additive oxygen content	Minor elements in additive
94.7	5.3	_
81.9	14.4	N (3.7 %)
84.1	15.4	S(0.5 %)
68.0	30.8	Si (0.6 %) S (0.6 %)
63.4	35.1	S (0.8 %) Cl (0.5 %)
	content 94.7 81.9 84.1 68.0	content content 94.7 5.3 81.9 14.4 84.1 15.4 68.0 30.8

Crystallite size =
$$\frac{k\lambda}{\beta\cos\theta}$$

Where K = 1.89 for La and 0.89 for Lc, β = full width at half max, λ = 1.5459 and θ = Bragg diffraction angle.

2.2.2. Transmission electron microscope (TEM) and selected area electron diffraction (SAED)

Transmission electron microscope samples were prepared by sonicating a few milligrams (mg) of graphitized material in ethanol and then a droplet of the suspension was placed on a copper (Cu) supported lacey carbon grid and allowed to dry. The samples were imaged using a FEI TalosTM F200X scanning/transmission electron microscope equipped with FEG source providing 0.12 nm resolution. The instrument was operated at 200 kV and the samples were imaged at various magnifications in the ranges. Selected area electron diffraction (SAED) patterns were taken concurrently with TEM imaging.

2.2.3. Raman spectroscopy

Raman spectra was collected using Horiba LabRAM HR Evolution equipped with 300 groove/mm grating and a 532 nm laser. The spectra were acquired in DuoScanTM mode which increases the statistical significance of the data by rastering over a wider area. At least 5 measurements were collected for each sample to ensure that the analysis was representative.

2.2.4. X-ray photoelectron spectroscopy (XPS)

a

XPS experiments were performed using a Physical Electronics VersaProbe II instrument equipped with a monochromatic Al K_{α} X-ray

source (h $\nu=1486.7$ eV) and a concentric hemispherical analyzer. Charge neutralization was performed using both low energy electrons (<5 eV) and argon ions. The binding energy axis was calibrated using sputter cleaned Cu (Cu $2p_{3/2}=932.62$ eV, Cu $3p_{3/2}=75.1$ eV) and Au foils (Au $4f_{7/2}=83.96$ eV). Peaks were charged with reference to C-C (sp²) band in the carbon 1 s spectra at 284.5 eV. Measurements were made at a takeoff angle of 45° with respect to the sample surface plane. This resulted in a typical sampling depth of 3–6 nm (95 % of the signal originated from this depth or shallower). Quantification was done using instrumental relative sensitivity factors (RSFs) that account for the X-ray cross section and inelastic mean free path of the electrons.

3. Results and discussion

Graphene oxide additives were first sonicated in methanol for dispersion [19,20]; then this sonicated solution was added before polymerization of the novolac phenolic resin (Fig. 1a). These additives were selected based on their oxygen content (Table 1 and Supporting Information Figs. S1 and S2) and their layered structures morphology as shown by transmission electron microscope (TEM) (Supporting Information Figs. S1 and S2). To determine the percentage weight (wt.%) of additive that gives the best graphitic quality, varied additive weight percentages were tested in the novolac matrix (N): 1, 1.75, 2.5, 3.5, and 5 wt.(%). X-ray diffraction (XRD) analysis was applied to determine the level of graphitization in graphitic materials. The best additive percent was gauged based on measuring the d(002) spacing wherein 2.5 wt.(%) was optimal. Fig. 1b and c show the d(002) values for RGO1-N and GPL-N . There is a decrease in d(002) spacing with an increase in additive wt.(%) up to 2.5 wt.(%) while an increase in the d(002) spacing

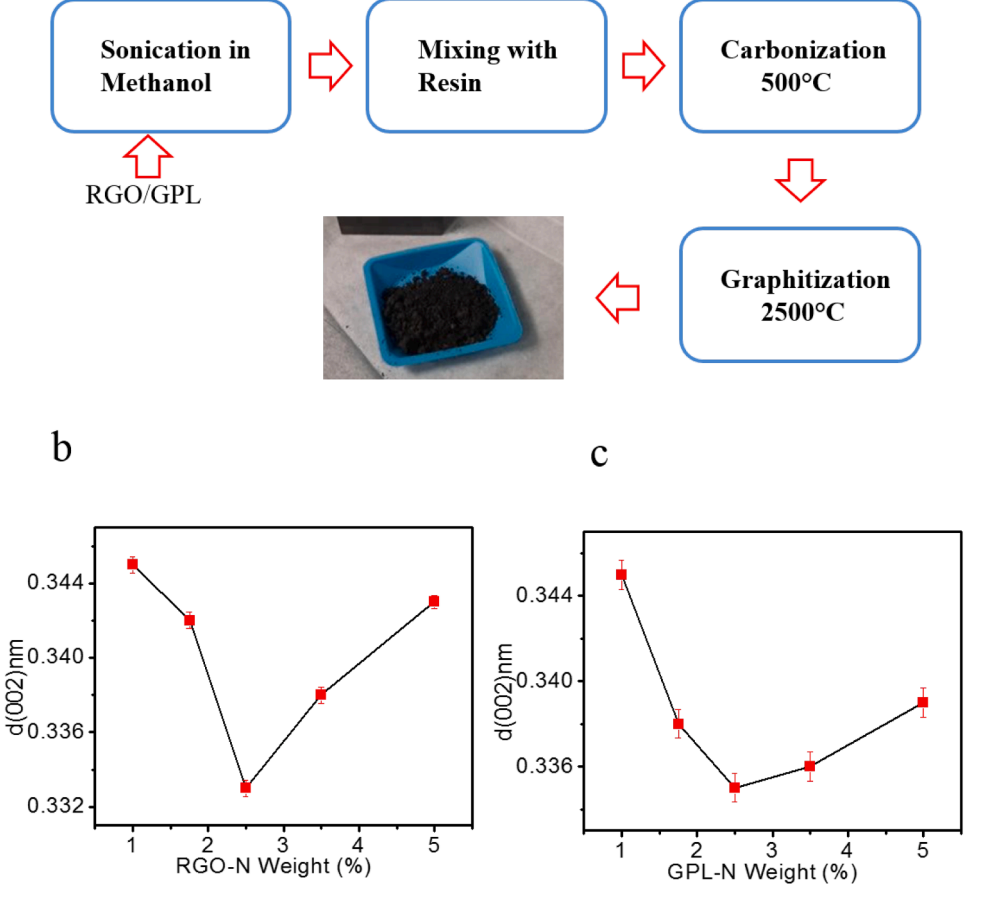


Fig. 1. (a) flowchart of experimental procedure; d(002) as a function of additive weight percent for (b) RGO1-N and (c) GPL-N.

was observed as the additive wt.(%) increased beyond 2.5 wt.(%). Therefore, the lowest d(002) spacing occurs at 2.5 wt.(%) and this was the optimal weight percent of additive to induce maximum graphitization in the novolac matrix. A similar trend was observed when crystallite height (Lc) and crystallite length (La) were measured; the maximum crystallite size occurs with 2.5 wt.(%) of GO additive (see supporting information, Fig. S3).

Fig. 2a and b shows the XRD spectra of 2500 °C heat treated novolac, GPL-N, RGO-N and GO-N samples of varied additive oxygen content. Pure novolac has a very broad peak d(002) peak (at $\sim 26^{\circ}$) consistent with a non-graphitizing carbon. Phenolic resins have been shown not to graphitize at HTTs even above 2500 $^{\circ}$ C. This is because they do not pass through a mesophase or crystalline formation stage during carbonization that allows stacking and growth of the carbon lamellae [21,22]. In contrast, GPL-N, RGO-N and GO-N samples with graphene oxide derivatives (<30.8at.% O content) show (002), (004) and (006) reflexes of the (001) series corresponding to ordered stacking along the c-axis samples. It appears that the addition of the graphene oxides (< 30.8at% O content) improves the graphitization of novolac at 2500 °C. The exception to this trend is GO2-N which shows a broad d(002) peak like that of pure novolac, therefore, pointing to a non-graphitizing characteristic of the GO2-N material. Further analysis using XRD parameters d (002), crystallite size La, and crystallite height Lc will help determine graphitization quality of the heat-treated materials.

Raman (Fig. 2c and d) shows a prominent p-band in spectra for pure novolac and GO2-N. The D-band at 1350 cm⁻¹ is the defect peak, which represents basal discontinuities (i.e., edges) and disorder of graphite layers [23,24]. A significant D-band as shown here translates to lattice defects in the heat-treated samples. On the contrary, heat-treated GPL-N, RGO-N and GO-N materials (< 30.8 % O content) show a reduced D-band or absence of D-band and a narrower G-band at 1580 cm⁻¹ indicating a higher graphitic quality. The G-band is the primary mode in graphene and graphite and represents the planar configuration sp2 bonded carbon [25,26]. Likewise, the 2D band (\sim 2700 cm⁻¹) of the GPL-N and RGO-N materials have a different shape compared to the GO-N and pure novolac materials. The 2D-band is the second order of the D-band, not representative of defects but can be used to determine the graphene layer thickness [25,26]. The shapes of RGO-N and GPL-N materials represent several layer thicknesses or an increase in layer thickness of graphene compared to GO-N and pure novolac whose shape represents a single or bilayer graphene thickness [25,26]. The I_D/I_G ratio was calculated to be 0.04 for GPL-N, 0.02 for both RGO-N materials and 0.07 for GO1-N while a higher value of 0.17 and 0.2 for the GO2-N and novolac materials, respectively. These findings from Raman are consistent with observations in the XRD spectra.

Further evidence of graphitization can be seen using transmission electron microscopy (TEM) (Figs. 3 and 4). Fig. 3 shows the TEM images of pure novolac, GPL-N and RGO1-N. Pure novolac (Fig. 3a-c), depicts

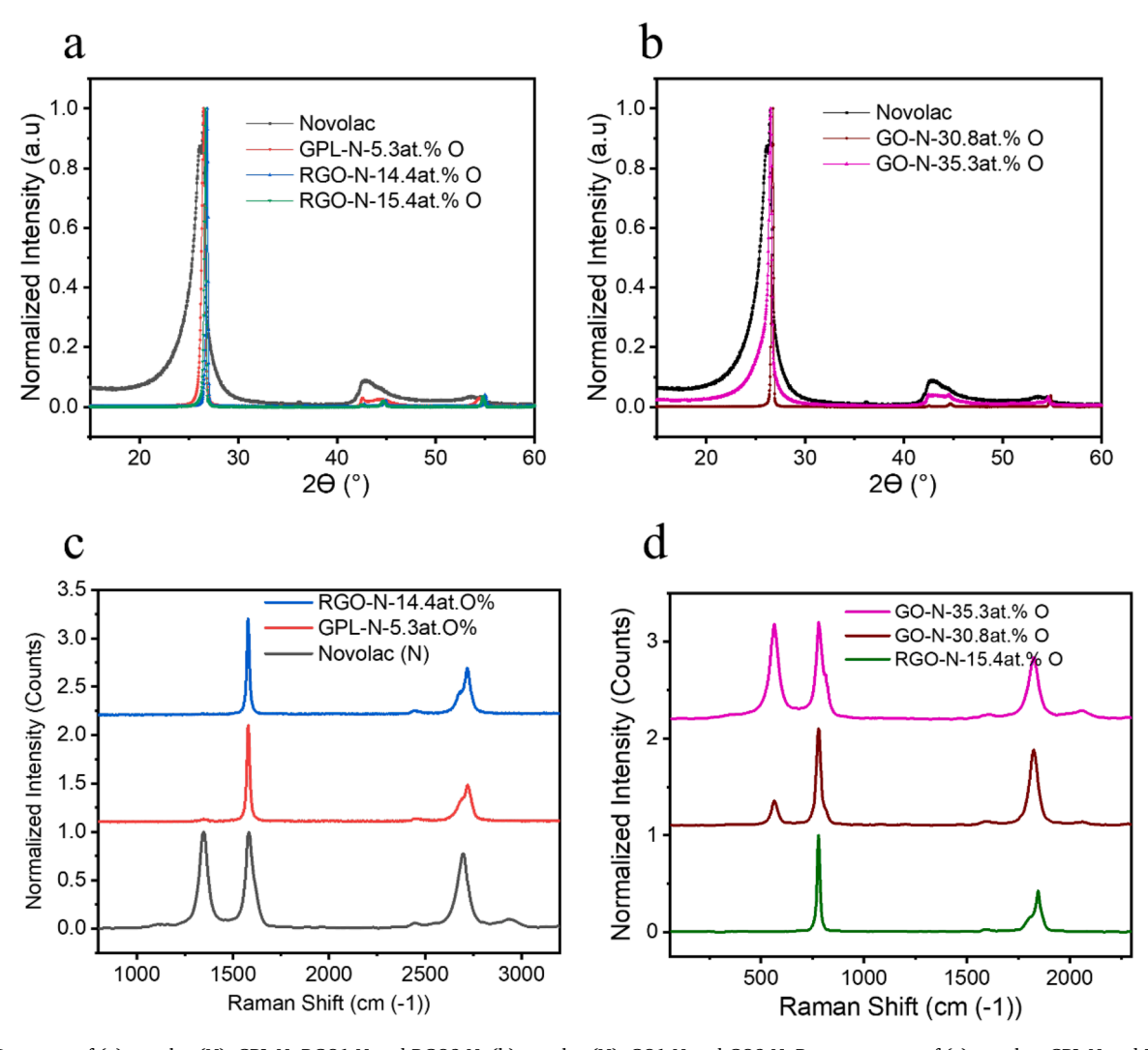


Fig. 2. XRD spectra of (a) novolac (N), GPL-N, RGO1-N and RGO2-N, (b) novolac (N), GO1-N and GO2-N; Raman spectra of (c) novolac, GPL-N and RGO1-N, (d) RGO2-N, GO1-N and GO2-N.

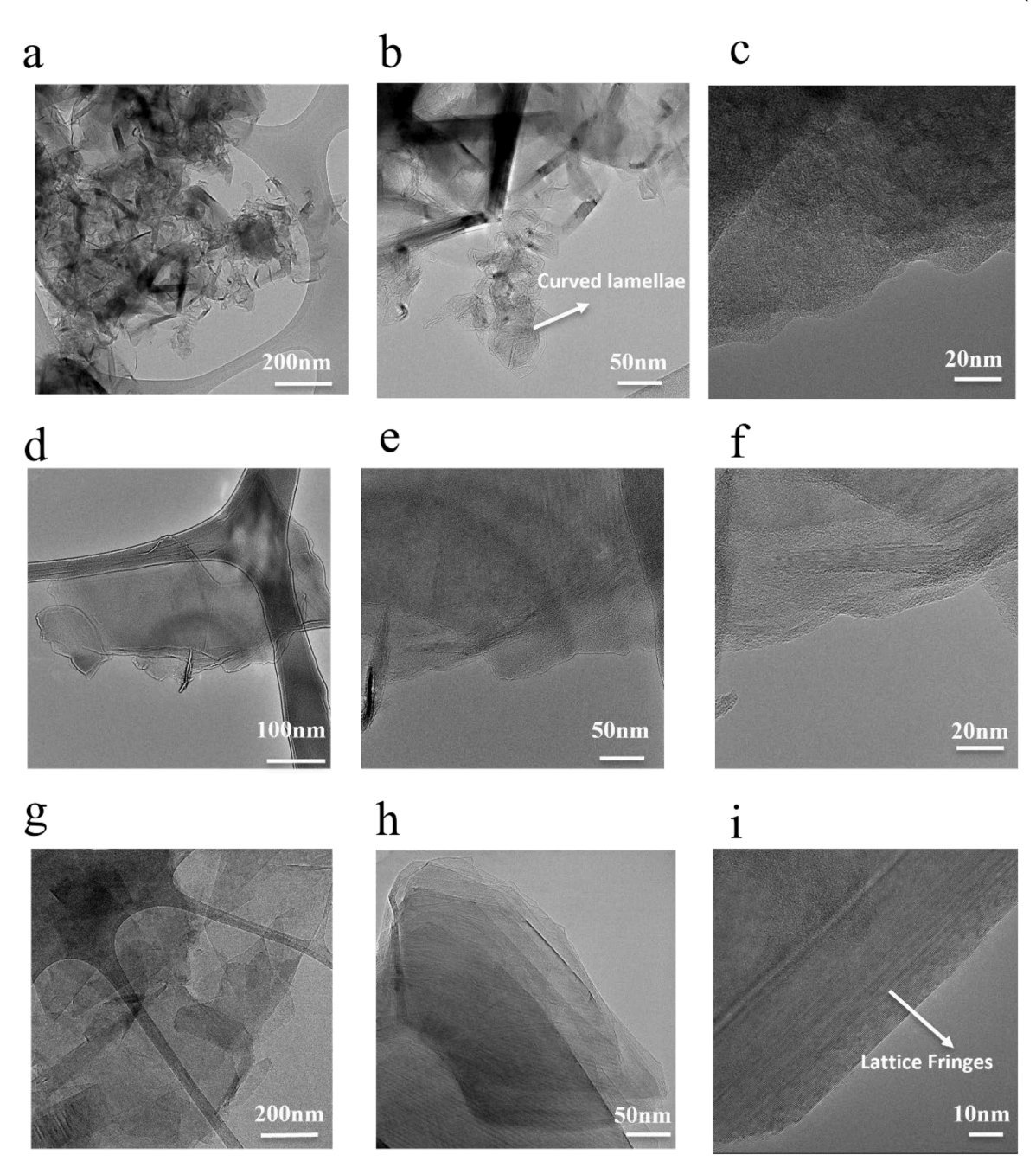


Fig. 3. Transmission Electron Microscope (TEM) images of novolac (N) (a-c), GPL-N (d-f), and RGO1-N (g-i).

curved and ribbon-like nanostructure, short range order, and indicative of a non-graphitizing matrix. However, the TEM images of GPL-N and RGO1-N, Fig. 3d–F and g–i respectively, illustrate improved nanostructure with sheet-like stacks and lattice fringes signifying long range order and indicative of a graphitizing material. This supports the hypothesis of templating interactions between the graphene oxide derived additives and novolac matrix leading to a change in the nanostructure and hence improved graphitic quality.

Further confirming templating interactions leading to the formation of highly graphitic structures is the TEM images of RGO2-N in Fig. 4a–c. A well-ordered nanostructure is depicted with clearly defined lattice fringes and sheet stacking like its counterpart RGO1-N in Fig. 3g–i. A lesser defined nanostructure appears in the TEM images of GO1-N Fig. 4d–f, while curved fullerenic- structures comparable to that of pure novolac are observed for GO2-N in Fig. 4g–i. It can be surmised that oxygen content in the GO additives play a role in the degree of

graphitization and that there is an optimum required to effect templating and influence the graphitic structure of the matrix.

Selected area electron diffraction (SAED) was used to further study the graphitization level of the materials. Fig. 5a shows the SAED patterns of the pure novolac sample where a mixture of amorphous and polycrystalline diffraction patterns is evidenced by diffused rings and presence of a few nano-crystallites. These nano-crystallites are formed during HTT of the resin (2500 °C). However, they do not imply long range order in the pure novolac matrix. Furthermore, TEM images of the pure resin (Fig. 3a–c) show lamellae curvature and ribbon-like structures (as seen in the 2D TEM projection) that are not characteristic of graphitized materials. A similar pattern can be seen in the GO2-N material in Fig. 5f. In contrast, the SAED image (Fig. 5c) of RGO1-N, shows concentric circles that correspond to multiple diffraction occurrences. This suggests that there are two or more graphenic sheet stacks on top of one another. As a result, a portion of the electron beam diffracted by the

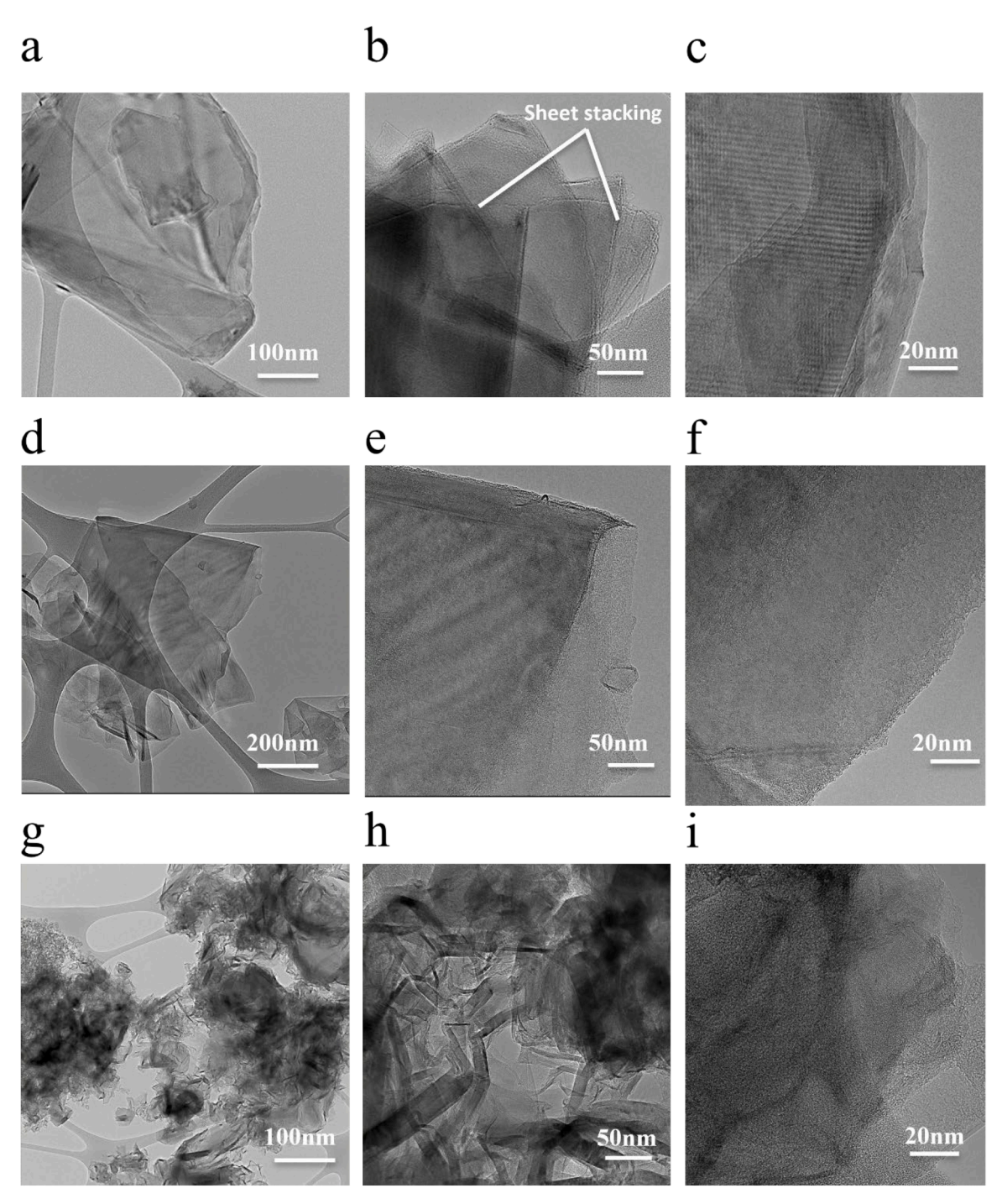


Fig. 4. Transmission Electron Microscope (TEM) of RGO2-N (a-c), GO1-N (d-f), and GO2-N (g-i).

first stack is diffracted by the second stack to manifest a double diffraction pattern; effectively the high intensity diffracted beams become the source beams for another set of layers. Such diffraction behavior is evidence of long-range order and the high graphitic quality of RGO1-N. Similarly, the RGO2-N SAED pattern (Fig. 5d) also indicates long range order, clearly showing the (101) planes. GPL-N SAED pattern (Fig. 5b) shows a polycrystalline pattern representing randomly oriented crystallites. It is observed that the GPL-N has a more improved crystalline pattern than the pure novolac but does not possess the high-level long-range order as seen in both RGO—N materials. The same is true for the SAED pattern (Fig. 5e) of GO1-N. These SAED patterns support results already seen in XRD, RAMAN and TEM analyses. In addition, the SAED pattern and TEM images of both RGO—N materials demonstrate

RGO as the best templating additive for novolac to obtain a high-quality graphitic material. It is therefore evident that GO and its derived additives are acting as templates to direct the matrix of pure novolac matrix from a non-graphitizing to a graphitizing one; however, there is a limit of oxygen content in GO additives to effect graphitization of the novolac matrix.

To further confirm the effect of oxygen groups as stated in the hypothesis, a comparison was made between the oxygen content of the graphene oxide additives and the graphitic quality of their corresponding heat-treated materials using XRD parameters d(002), Lc and La. The D-spacing value is a primary measure of graphitic quality. Fig. 6a shows the d(002) trend with percentage oxygen content of graphene oxide additive. The plot shows d(002) decreases with increase in

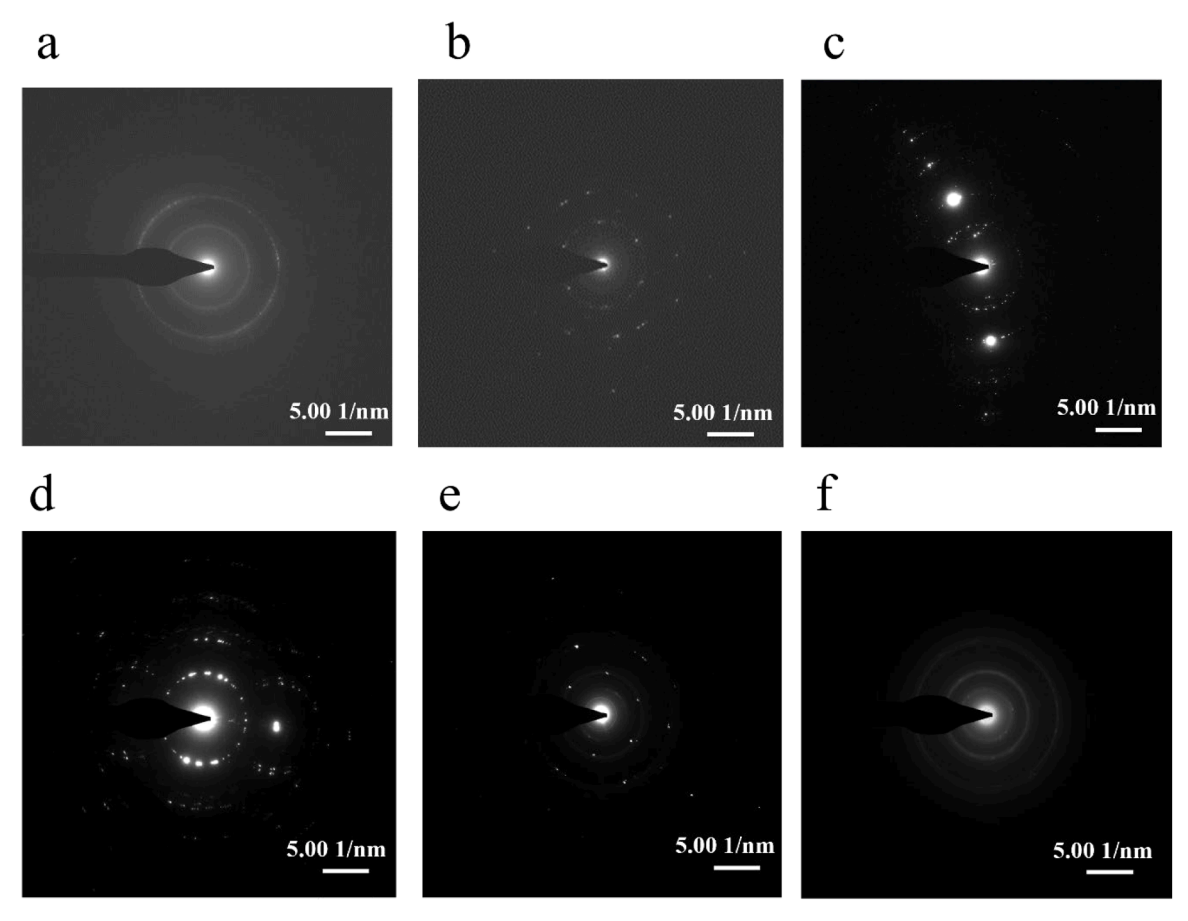


Fig. 5. Selected area electron diffraction (SAED) pattern of (a) Novolac (N) (b) GPL-N, (c) RGO1-N, (d) RGO2-N, (e) GO1-N, (f) and GO2-N.

percentage oxygen content up to 15.4 at.(%) O and begins to increase as oxygen content (in GO) increases beyond 15.4 at.(%). Pure novolac with no GO additive (i.e., zero added% oxygen content) has a d(002) value of 0.336 nm, while GPL-N (5.3 at.(%) O) has a d(002) spacing of 0.335 nm. Ultimately, RGO—N materials (14.4 at.(%) and 15.4 at.(%) O) have the smallest D-spacing of 0.334 nm. An increase in D-spacing to 0.336 nm and 0.337 nm was measured in the GO1-N and GO2-N samples with high O content of 30.8 at.(%) and 35.3 at.(%), respectively. These results indicate more specifically that there is a positive correlation between an increase in graphitic quality and oxygen content in GO derived additives \leq 15.4 at.(%) O. Beyond 15.4 at.(%) O content, a negative correlation occurs and the level of graphitic quality decreases.

Likewise, the presence of oxygen functional groups on graphene oxide (GO) has been shown to improve the graphitization of phenolic resins elsewhere [24-26]. In a related study, a very small concentration (0.1 wt.(%) of GO) in phenolic carbon-carbon composites served as a nucleating agent leading to the formation of graphitic structure. That study found that the oxygen-containing functional groups on the GO played a significant role in enhancing the interfacial reactions between the GO and phenolic resin matrix and improved graphitization of the composite (24). The improved GO-novolac matrix interactions occur through the esterification reaction as well as the π - π stacking overlap between the GO and phenolic units in the matrix [25]. In molecular dynamics simulations, Papkov et al. [27], identified a templating effect of GO upon the graphitic structure of continuous carbon nanofibers made from polyacrylonitrile (PAN). Fibers containing GO (1.4 wt.(%)) showed significantly improved graphitic order compared to the pristine fibers which was attributed to a templating effect of the GO that caused formation of preferentially oriented graphitic crystallites.

Operationally, in the present study, with more oxygen groups, there are more radical sites formed for bonding with the matrix and better

alignment of the matrix derived cyclic and aromatic structures aided by the π -electron network and pseudo-two-dimensional morphology of the GO additives. This is observed for up to 15.4 at.(%) O content in GO additive. Thereafter, larger amounts of oxygen groups lead to a disrupted sp² framework and cannot effectively act as a template to direct and align the structure of matrix from a non-graphitizing to a graphitizing one.

Furthermore, lattice parameters (La and Lc) plotted versus percentage oxygen content show similar results as d(002) (Fig. 6b, c). Large Lc and La values indicate a high degree of graphitization (or better graphitic quality). While pure novolac has La and Lc values of 28 nm and 26 nm, a sharp increase was seen in the La and Lc values to 126 nm and 35 nm, respectively, for GPL-N (5.4 at.(%) O). The highest values for La and Lc were measured for RGO-N materials which have values of 135 nm and 39 nm for RGO1-N (14.4 at.(%) O) and paralleled by RGO2-N (15.4 at.(%) O) values of, 141 nm and 41 nm. Lastly, the La and Lc values for GO1-N (30.8 at.(%) O) are 70 nm and 24 nm, respectively. Correspondingly, the lowest values of 11 nm and 8 nm were measured for GO2-N (35.3 at.(%) O). Therefore, these results show that there is a positive correlation between an increase in graphitic quality and oxygen content in GO derived additives ≤ 15.4 at.(%) O. Beyond 15.4 at.(%) O content, a negative correlation occurs and the level of graphitic quality decreases.

4. Templating mechanism of novolac by graphene oxide additives

In this work, GO-derived additives are shown to induce graphitization of novolac (a non-graphitizing precursor) by templating. Additionally, it was found that the templating mechanism also depends on the matrix. For instance, novolac appears to respond well (graphitize)

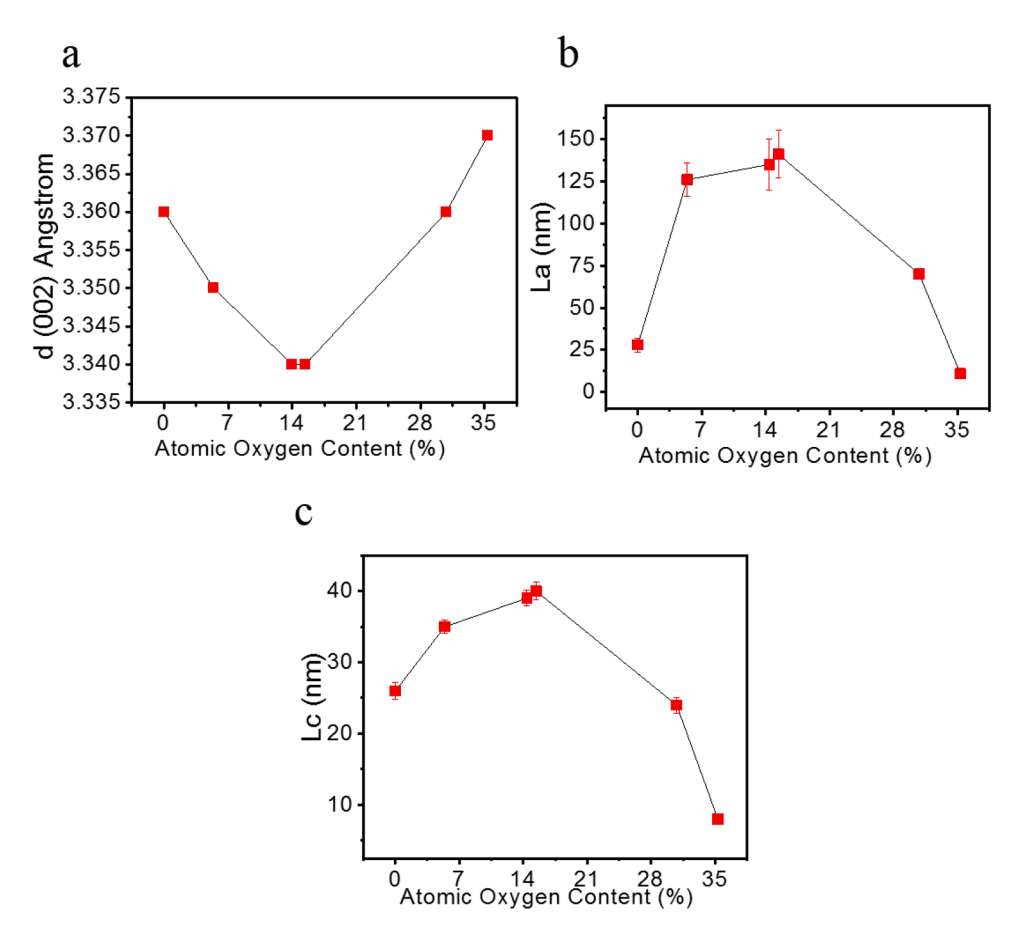


Fig. 6. Lattice parameters extracted from deconvoluted XRD spectra of novolac (N), GPL-N (5.3at.% O), RGO1-N (14.4at.% O), RGO2-N (15.4at.% O), GO1-N (30.8at.% O) and GO2-N (35.3at.% O) vs.%oxygen content of the additives (a) d (002) versus%oxygen content (b) La versus%oxygen content (c) Lc versus%oxygen content.

when RGO is added.

To identify the chemical interactions between the GO materials and novolac, an alternative configuration was implemented. Thin films of novolac (N), RGO1-N, and GPL-N were made by doctor blading and rapidly inserted into a furnace pre-heated to 300 °C. FT-IR analysis was conducted on the films to gain insight on reactions that occur between the GO additives and the matrix. Based on the spectroscopic analysis for this early stage of carbonization, a possible mechanism for the templating induced graphitization of novolac by graphene oxide derivatives is proposed. For chemical templating to occur, oxygen functional groups of the GO additives leave during carbonization to form radical sites for bonding with the decomposing matrix. Upon exposure to 300 °C, novolac polymerization reactions occur, [28] forming intermediate structures such as hydroxymethyl phenol as seen in Fig. 7a. The methylol group (C-OH) of hydroxymethyl phenol may undergo condensation reactions to form CH₂ linkages. Similarly, the methylol group may also react with the oxygen functional groups of GO derivatives. From XPS analysis, the oxygen functional groups detected in the GO additives were -O-C=O, C=O, and C-O. The -O-C=O group is known to populate the edge sites, which will be the more reactive site for bonding of the

In the FT-IR spectra (Fig. 7b), the -OH group (at $\sim 3500 {\rm cm}^{-1}$) decreases for RGO1-N and GPL-N compared to pure novolac. The expectation here is that the methylol group from novolac reacts with the -COOH group of the GO derived additives leading to a loss of -OH group in the form of water resulting in an ester coupling. The bands at 1730 cm⁻¹ and 1250 cm⁻¹ (Fig. 7c) are attributed to both stretching of C=O and C-O of the ester groups that reveals formation of methyl ester via covalent bonding. This evidence supports the bonding that takes place

between the novolac matrix and GO additive which is necessary for reactive templating upon HTT.

Meanwhile, the two-dimensional morphology of the GO derived additives could also play a role in graphitization through $\pi-\pi$ interactions with the novolac matrix as identified by ReaxFF modeling. Experimentally this has been referred to as 'confinement' or structure-directing graphitization [29]. Huang et al. used graphene with no oxygen functional groups to induce graphitization of polyacrylonitrile (PAN) resulting in highly crystalline graphite films. This result suggests that the ${\rm sp}^2$ network of the GO additives contributes to aromatic ring alignment in the adjacent matrix. In the present work, the combined contributions of chemical and physical templating were manifested in the improved graphitic quality GO derived-novolac materials compared to pure novolac.

5. Conclusion

In this work, a technique to convert non-graphitizable precursors into graphitizable ones by the addition of graphene oxide and its derivatives was demonstrated. It was shown that the addition of additives with oxygen content $\geq\!15.4$ at.(%) to the novolac matrix can lead to highly graphitic material after high temperature treatment (2500 °C). XRD analysis showed the decrease of d(002) and increase of crystallite size (La) and crystallite height (Lc) for GPL-N and RGO-N materials ($\geq\!15.4$ at.(%) O). In addition, RGO—N materials of similar additive oxygen content (15.4 at.% and 14.4 at.%) gave parallel results and showed the best graphitic quality after HTT as measured by XRD. Results of improved graphitization caused by the addition of the GO derived additive were supported by Raman and TEM characterizations. The

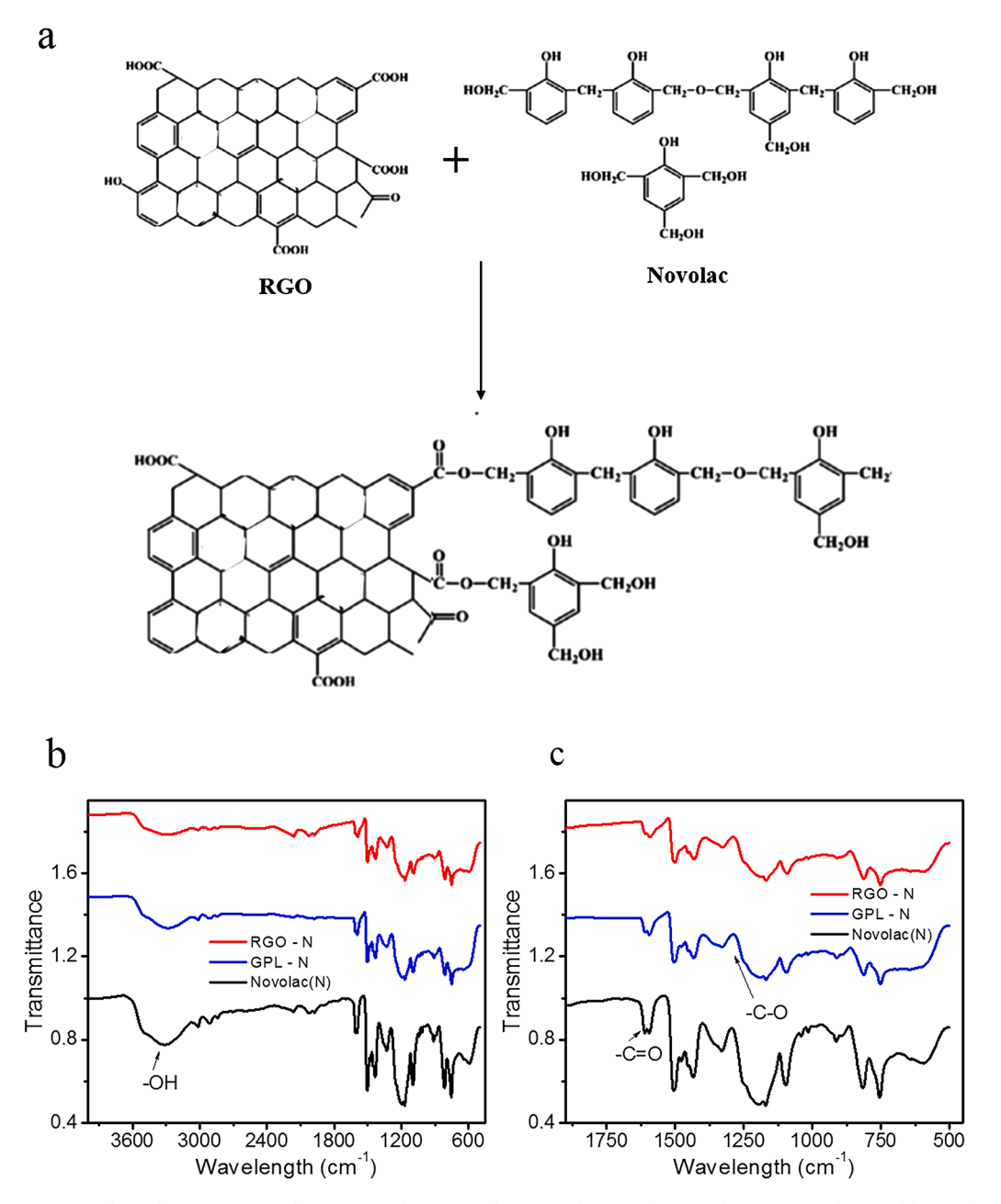


Fig. 7. (a) Basic novolac polymerization mechanism [28] (b, c) FTIR showing reduction of -OH and -C-O groups due to addition of additives.

working hypothesis is that these GO derived additives act as chemical and physical templates to induce the graphitization of the novolac matrix. Chemical templating occurs as oxygen groups of the GO derived additives form reactive radicals that provide bonding to the decomposing novolac matrix. Also, aromatic rings formed during carbonization of novolac align with the sp² network of the two-dimensional graphene oxides, thereby aiding in the formation of layered graphite material, a process called physical templating. Lastly, the results show there is an optimum amount of oxygen content in GO additives needed to induce graphitization of the novolac matrix as XRD results show the addition GO additive of higher oxygen content (≥ 30.8 % O) to the novolac matrix (GO-N) led to poor graphitic quality after HTT. This is attributed to large amounts of oxygen groups which create a disrupted sp² framework and cannot effectively act as a template to direct and align the structure of matrix from a non-graphitizing to a graphitizing one. This work is important because of the current need for graphitic materials, especially for energy storage applications. Additionally, the templating technique could be a more environmental and cost-effective method to turn non-graphitizing precursors into graphitizable ones.

CRediT authorship contribution statement

Sandra N Ike: Data curation, Formal analysis, Investigation, Methodology, Writing – original draft, Writing – review & editing. **Randy Vander Wal:** Conceptualization, Funding acquisition, Methodology, Resources, Supervision, Writing – review & editing.

Declaration of competing interest

The authors declare that they have no known competing financial interests or personal relationships that could have appeared to influence the work reported in this paper.

Data availability

No data was used for the research described in the article.

Acknowledgment

This material is based upon work supported by the National Science Foundation under Grant No. (2306042). Acknowledgment is also made to the donors of the American Chemical Society Petroleum Research Fund for support of this research.

Supplementary materials

Supplementary material associated with this article can be found, in the online version, at doi:10.1016/j.cartre.2024.100388.

References

- B.P. Thapaliya, H. Luo, P. Halstenberg, H.M. Meyer, J.R. Dunlap, S. Dai, Low-cost transformation of biomass-derived carbon to high-performing nano-graphite via low-temperature electrochemical graphitization, ACS Appl. Mater. Interfaces 13 (2021) 4393–4401, https://doi.org/10.1021/acsami.0c19395.
 A. Wang, J. Ren, B. Shi, G. Lu, Y. Wang, A facile one-pot synthesis of mesoporous
- [2] A. Wang, J. Ren, B. Shi, G. Lu, Y. Wang, A facile one-pot synthesis of mesoporous graphite-like carbon through the organic-organic co-assembly, Microporous Mesoporous Mater. 151 (2012) 287–292, https://doi.org/10.1016/j. micromeso.2011.10.022.
- [3] Y. Nakamura, T. Yoshino, M. Satish-Kumar, Pressure dependence of graphitization: implications for rapid recrystallization of carbonaceous material in a subduction zone, Contrib. Minerl. Petrol. 175 (2020) 1–14, https://doi.org/10.1007/s00410-020-1667-2.
- [4] K. Li, J. Zhang, Y. Liu, M. Barati, Z. Liu, J. Zhong, B. Su, M. Wei, G. Wang, T. Yang, Graphitization of coke and its interaction with slag in the hearth of a blast furnace, Metall. Mater. Trans. B Process Metall. Mater. Process. Sci. 47 (2016) 811–818, https://doi.org/10.1007/s11663-015-0574-9.
- [5] Z. Guo, K. Jiao, J. Zhang, H. Ma, S. Meng, Z. Wang, J. Zhang, Y. Zong, Graphitization and performance of deadman coke in a large dissected blast furnace, ACS Omega 6 (2021) 25430–25439, https://doi.org/10.1021/acsomega.1c03398.
- [6] H.F. Arani, A.R. Mirhabibi, S. Collins, R. Daroughegi, A. Khalife Soltani, R. Naghizadeh, N. Riahi-Noori, R. Aghababazadeh, A. Westwood, Enhancement in graphitization of coal tar pitch by functionalized carbon nanotubes, RSC Adv. 7 (2017) 5533–5540, https://doi.org/10.1039/c6ra25441a.
- [7] M. Gubernat, T. Lis, J. Tomala, J. Kawala, A. Fraczek-Szczypta, S. Blazewicz, Study of the carbonization and graphitization of coal tar pitch modified with SiC nanoparticles, J. Nanomater. (2017) 2017, https://doi.org/10.1155/2017/ 6578028
- [8] S.R. Sivakkumar, J.Y. Nerkar, A.G. Pandolfo, Rate capability of graphite materials as negative electrodes in lithium-ion capacitors, Electrochim. Acta 55 (2010) 3330–3335, https://doi.org/10.1016/j.electacta.2010.01.059.
- [9] H. Zheng, M.S. Kim, Performance of modified graphite as anode material for lithium-ion secondary battery, Carbon Lett. 12 (2011) 243–248, https://doi.org/ 10.5714/CL.2011.12.4.243.
- [10] E. Peled, Improved graphite anode for lithium-ion batteries chemically, J. Electrochem. Soc. 143 (1996) L4, https://doi.org/10.1149/1.1836372.
- [11] L. Ma, I. Jia, X. Guo, L. Xiang, High performance of Pd catalysts on bimodal mesopore for the silica catalytic oxidation of toluene, Chin. J. Catal. 35 (2014) 108–119, https://doi.org/10.1016/S1872.
- [12] X. Dou, I. Hasa, D. Saurel, C. Vaalma, L. Wu, D. Buchholz, D. Bresser, S. Komaba, S. Passerini, Hard carbons for sodium-ion batteries: structure, analysis, sustainability, and electrochemistry, Mater. Today 23 (2019) 87–104, https://doi. org/10.1016/j.mattod.2018.12.040.

- [13] L.J. Lanticse-Diaz, Y. Tanabe, T. Enami, K. Nakamura, M. Endo, E. Yasuda, The effect of nanotube alignment on stress graphitization of carbon/carbon nanotube composites, Carbon 47 (2009) 974–980, https://doi.org/10.1016/j.carbon.2008.11.046. N. Y.
- [14] B. Reznik, M. Guellali, D. Gerthsen, R. Oberacker, M.J. Hoffmann, Microstructure and mechanical properties of carbon-carbon composites with multilayered pyrocarbon matrix, Mater. Lett. 52 (2002) 14–19, https://doi.org/10.1016/S0167-577X(01)00357-3
- [15] S.S. Tzeng, Y.H. Lin, Formation of graphitic rods in carbon/carbon composites reinforced with carbon nanotubes, Carbon 52 (2013) 617–620, https://doi.org/ 10.1016/j.carbon.2012.10.010, N. Y.
- [16] B. Saha, A. Furmanchuk, Y. Dzenis, G.C. Schatz, Multi-step mechanism of carbonization in templated polyacrylonitrile derived fibers: reaxFF model uncovers origins of graphite alignment, Carbon 94 (2015) 694–704, https://doi.org/ 10.1016/j.carbon.2015.07.048, N. Y.
- [17] Z. Gao, J. Zhu, S. Rajabpour, K. Joshi, M. Kowalik, B. Croom, Y. Schwab, L. Zhang, C. Bumgardner, K.R. Brown, D. Burden, J.W. Klett, A.C.T. van Duin, L.V. Zhigilei, X. Li, Graphene reinforced carbon fibers, Sci. Adv. 6 (2020) 1–11, https://doi.org/ 10.1126/sciadv.aaz4191.
- [18] Y. Ma, Y. Yang, C. Lu, X. Wen, X. Liu, K. Lu, S. Wu, Q. Liu, Extraordinary improvement of ablation resistance of carbon/phenolic composites reinforced with low loading of graphene oxide, Compos. Sci. Technol. 167 (2018) 53–61, https://doi.org/10.1016/j.compscitech.2018.07.026.
- [19] Y. Guo, X. Sun, Y. Liu, W. Wang, H. Qiu, J. Gao, One pot preparation of reduced graphene oxide (RGO) or Au (Ag) nanoparticle-RGO hybrids using chitosan as a reducing and stabilizing agent and their use in methanol electrooxidation, Carbon 50 (2012) 2513–2523, https://doi.org/10.1016/j.carbon.2012.01.074. N. Y.
- [20] F. Pendolino, G. Capurso, A. Maddalena, S.Lo Russo, The structural change of graphene oxide in a methanol dispersion, RSC Adv. 4 (2014) 32914–32917, https://doi.org/10.1039/c4ra04450a.
- [21] P. Ouzilleau, A.E. Gheribi, P. Chartrand, G. Soucy, M. Monthioux, Why some carbons may or may not graphitize? The point of view of thermodynamics, Carbon 149 (2019) 419–435, https://doi.org/10.1016/j.carbon.2019.04.018. N. Y.
- [22] K.K. Jenkins GM, Polymeric Carbons: Carbon Fibre, Glass and Char, Cambridge University Press, London, 1976.
- [23] K.N. Kudin, B. Ozbas, H.C. Schniepp, R.K. Prud'homme, I.A. Aksay, R. Car, Raman spectra of graphite oxide and functionalized graphene sheets, Nano Lett. 8 (2008) 36–41, https://doi.org/10.1021/nl071822v.
- [24] S. Stankovich, D.A. Dikin, R.D. Piner, K.A. Kohlhaas, A. Kleinhammes, Y. Jia, Y. Wu, S.T. Nguyen, R.S. Ruoff, Synthesis of graphene-based nanosheets via chemical reduction of exfoliated graphite oxide, Carbon 45 (2007) 1558–1565, https://doi.org/10.1016/j.carbon.2007.02.034. N. Y.
- [25] K.I. Sasaki, Basic principles of Raman spectroscopy for graphene, NTT Tech. Rev. 11 (2013) 1–5. https://www.ntt-review.jp/archive/ntttechnical.php?contents=nt r201308fa2.pdf&mode=show pdf.
- [26] D. Němeček, G.J. Thomas, Raman spectroscopy of viruses and viral proteins, Front. Mol. Spectrosc. (2008) 553–595, https://doi.org/10.1016/B978-0-444-53175-9.00016-7.
- [27] D. Papkov, A. Goponenko, O.C. Compton, Z. An, A. Moravsky, X.Z. Li, S.T. Nguyen, Y.A. Dzenis, Improved graphitic structure of continuous carbon nanofibers via graphene oxide templating, Adv. Funct. Mater. 23 (2013) 5763–5770, https://doi. org/10.1002/adfm.201300653.
- [28] P.W. Kopf, E.R. Wagner, U.C. Corporation, formation and cure of novolacs: NMR study of transient molecules, J. Polym. Sci. 11 (1973) 939–960.
- [29] H. Huang, X. Ming, Y. Wang, F. Guo, Y. Liu, Z. Xu, L. Peng, C. Gao, Polyacrylonitrile-derived thermally conductive graphite film via graphene template effect, Carbon 180 (2021) 197–203, https://doi.org/10.1016/j. carbon.2021.04.090. N. Y.